Article

Interdiffusion in Zr-Mo/W Intermetallics

Kaihua Wang [1], Xingwei Liu [1,*], Tianyu Liu [1], Chuan He [1,2] and Jinxu Liu [1,2,*]

[1]   School of Materials Science and Engineering, Beijing Institute of Technology, Beijing 100081, China;
      18931075139@163.com (K.W.); bitlty123@163.com (T.L.); chuan.he@bit.edu.cn (C.H.)
[2]   China National Key Laboratory of Science and Technology on Materials under Shock and Impact,
      Beijing Institute of Technology, Beijing 100081, China
*   Correspondence: xwliu@bit.edu.cn (X.L.); liujinxu@bit.edu.cn (J.L.)

Abstract: Intermetallic compounds or solid solutions can form between Zr and Mo/W, in which the multiphase of the diffusion may be influenced by each other. Interdiffusion kinetic data in such intermetallic systems are highly demanded for material design. In this work, solid–solid diffusion couples of Zr-Mo and Zr-W were prepared by the fixture method, and the interdiffusion behaviors of Zr-Mo and Zr-W at 1300–1500 °C were systematically investigated. The results showed that the intermetallic compounds Mo_2Zr/W_2Zr formed in the Zr-Mo/W diffusion systems. The growth constants of the Mo_2Zr and W_2Zr phases varied with temperature in accordance with the Arrhenius relationship, and the activation energies of growth were 109 kJ/mol and 285 kJ/mol, respectively. In addition, (Zr, Mo) solid solution formed between Mo_2Zr and pure Zr as diffusion proceeded, resulting in a lower chemical potential for the formation of Mo_2Zr. The den Broeder method was used in calculating the interdiffusion coefficients of the solid solution. The results showed that the interdiffusion coefficient in the (Zr, Mo) solid solution decreased with the increase of Mo concentration. Moreover, the diffusion activation energy of the solid solution was evaluated based on the Arrhenius relationship, and the activation energy was 145–170 kJ/mol when the Mo content was in the range of 2–10 at. %. These diffusion kinetic data provide a reference for the composition design and preparation technic of Zr-based alloys.

Keywords: diffusion couple; Zr-based alloys; interdiffusion coefficients; activation energy

1. Introduction

Zirconium and its alloys are extensively used in the nuclear industry, chemical industry, aerospace, and biomedical fields because of their comprehensive properties, such as small thermal neutron absorption cross-section, high radiation resistance, excellent corrosion resistance, and mechanical properties [1–3]. To enhance the high-temperature performance of Zr alloys for complex application environments, refractory elements with high melting points are often added to Zr alloys [4–6]. The composition design of the alloy requires large and accurate diffusion kinetic databases. Fundamental kinetic data such as diffusion coefficients, growth constants, and activation energies are significant references for the analysis and prediction of phase transformation, microstructure formation, and performance modulation in alloys [7].

In addition, due to the high melting point of Zr-based refractory alloys and the different shapes of the alloys used in various applications, the materials prepared by conventional melting methods have problems such as poor uniformity of microstructure and difficulty in secondary processing. To solve these problems, the technique of powder metallurgy for the preparation of refractory metals and alloys was gradually developed. Powder metallurgy is a preparation technique in which high-purity metal powder is used as raw material, and the final products are produced without secondary processing or with less processing through powder mixing, press molding, and high-temperature sintering. This technique has the advantages of short process flow and near-net forming, which can achieve low-cost

and high-efficiency production of Zr-based refractory alloys [8]. Diffusion is the only and irreversible form of material migration in the solid phase sintering process of powder metallurgy, where the atoms and molecules are constantly moving from one position to another due to thermal movement. The microstructure of the material is formed by the diffusion of elements. To achieve sintered densification of the Zr alloys, the crucial point is to promote interdiffusion between the elements [9,10]. Therefore, knowledge of the diffusion behavior of elements is essential for the design of powder metallurgical processes.

In the past decades, some studies have reported the interdiffusion of Zr with other refractory elements [11–19]. Thibon et al. [14] analyzed the interdiffusion behavior of Zr-Ti alloys in the β-phase region and obtained the activation energy of diffusion in the Zr-Ti system. Wang et al. [18] prepared Zr-Nb, Zr-Hf, and Zr-Ta diffusion couples and calculated the interdiffusion coefficients of the three binary systems from 950 °C to 1200 °C, the results showed that the variation of the interdiffusion coefficients with temperature for Zr-Nb, Zr-Hf, and Zr-Ta systems were in accordance with the Arrhenius relationship. Prasad et al. [19] calculated the interdiffusion coefficients of the Zr-Nb binary system at different elemental concentrations between 1000 °C and 1200 °C, the results showed that the interdiffusion coefficients decreased with the increase of Nb content. These were all reports on diffusion kinetics in Zr-based binary solid solution systems. However, for the Zr-Mo and Zr-W binary systems, relevant reports were quite lacking, especially at high temperatures [20]. Zr-Mo/W alloys are commonly used as nuclear fuel cladding materials or reactive structural materials due to their high density, radiation resistance, high strength, and good oxidized reactivity with oxygen [5,6,21,22]. The binary phase diagram indicated that the intermetallic compounds Mo_2Zr and W_2Zr were formed in Zr-Mo and Zr-W systems [23,24]. The diffusion with the formation of new phases was called multiphase diffusion, which was typically characterized by the discontinuous concentration distribution in the diffused region. In addition, diffusion in intermetallic compounds and solid solutions may affect each other. Therefore, it is crucial to study and analyze the interdiffusion behavior of the Zr-Mo/W binary system.

In this work, to elucidate the influence mechanism of the solid solution and intermetallic phases during diffusion, and establish the diffusion kinetic data at high temperatures, we systematically investigated the interdiffusion behaviors of the Zr-Mo/W at 1300–1500 °C by the solid–solid diffusion couple method. Firstly, the Zr-Mo/W diffusion couple methods were set up to be used in annealing at 1300 °C, 1400 °C, and 1500 °C. Then, the elemental distribution of the diffused region was tested, and the diffusion kinetic data were calculated. Finally, the diffusion behavior of Zr-Mo and Zr-W binary systems was systematically investigated and discussed.

2. Materials and Methods

Zr, Mo, and W metals with 99.99 wt.% purity were used as raw materials. The solid–solid diffusion couples were prepared by the fixture method, and the fixture was prepared with high melting point metals to ensure that the fixture would not melt during the diffusion process at high temperatures. Then, the pure metal blocks were cut into $\Phi6 \times 6$ mm cylindrical specimens, and the diffused surface was polished to a mirror to obtain a smooth and bright surface. The samples were ultrasonically cleaned in anhydrous ethanol 2–3 times, then put into a vacuum thermostatic desiccator and dried at low temperature.

The treated samples were fixed as Zr-Mo and Zr-W diffusion couples by fixtures, and the diffusion surfaces between the samples were completely contacted as shown in Figure 1. Two groups of the same diffusion couples were set up as control experiments to reduce the experimental error. The diffusion couple samples were placed in a tubular resistance furnace with a protective atmosphere of pure Ar gas. Diffusion annealing was performed at 1300 °C, 1400 °C, and 1500 °C for 5 h. After annealing, the diffusion couples were removed and cut flat along the axial direction. Then, the samples were mounted in epoxy resin, and the surface was polished to a mirror by using 0.06 μm SiO_2 solution to facilitate microstructure observation and composition testing of the diffused region.
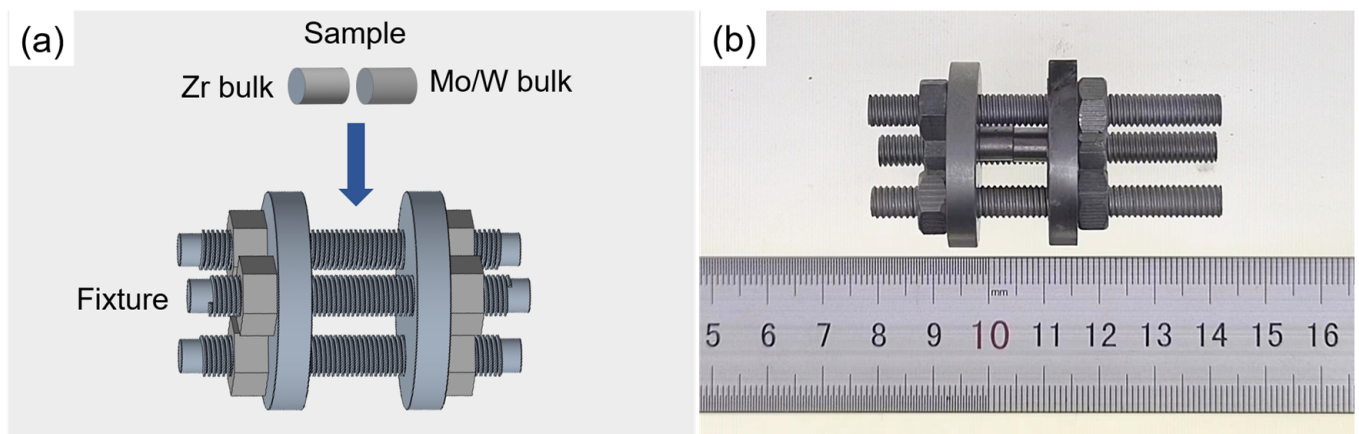
Figure 1. (**a**) Design drawing and (**b**) physical photograph of the diffusion couple.

The microstructure and concentration distribution in the diffused region were analyzed by scanning electron microscope (SEM, Gemini SEM 300, Zeiss, Jena, Germany) equipped with energy-dispersive X-ray spectroscopy (EDX, Aztec X-max 50, Oxford Instruments, Abingdon, UK). Firstly, the diffused regions of the Zr-Mo and Zr-W systems at 1300 °C, 1400 °C, and 1500 °C were determined by quantitative microzone analysis of EDX. Then, the concentration of the element was analyzed by using elemental content tests with equidistant fixed points along the diffusion direction. Finally, the concentration distribution curve was obtained by non-linear curve fitting of the data points obtained from the quantitative analysis.

3. Results and Discussion

3.1. Elemental Distribution State of the Diffused Region

In this section, to investigate whether the solid solution phase or intermetallic compound phase was formed in the Zr-Mo and Zr-W binary systems during the diffusion process, the elemental distribution states in the diffused regions of the Zr-Mo and the Zr-W binary systems at 1300 °C, 1400 °C, and 1500 °C, respectively, are determined by quantitative analysis of EDX.

3.1.1. Zr-Mo Binary System

Figure 2(a1) shows the BSE image and EDX-mapping of the entire diffused region determined by EDX quantitative analysis for the Zr-Mo diffusion system after annealing at 1300 °C for 5 h.

The quantitative analysis of the diffused region by EDX indicated that there were four regions in the Zr-Mo system. Sequentially, they were pure Zr, (Zr, Mo) solid solution phase, Mo_2Zr phase, and pure Mo. The thickness of the solid solution region was about 297 μm. Between the solid solution phase and the pure Mo phase, there was a very thin layer of Mo_2Zr with a thickness of about 4.48 μm. The wavy interface appeared at the interface between Mo_2Zr and (Zr, Mo) solid solution, which may be due to the anisotropy of diffusion leading to an uneven interface. Moreover, the existence of a small number of impurities in the raw material sample resulted in different energy barriers for the diffusion of atoms at different positions, which may also cause the formation of undulating phase interfaces.

The curves of concentration distribution of the solid solution phase (region 1) and Mo_2Zr phase (region 2), as shown in Figure 2(a2), were obtained by fitting and smoothing data from EDX quantitative analysis. The concentration of Mo elements in the solid solution varied continuously from 0 to 10 at. %, and the Mo content in the Mo_2Zr phase was about 66 at. %.
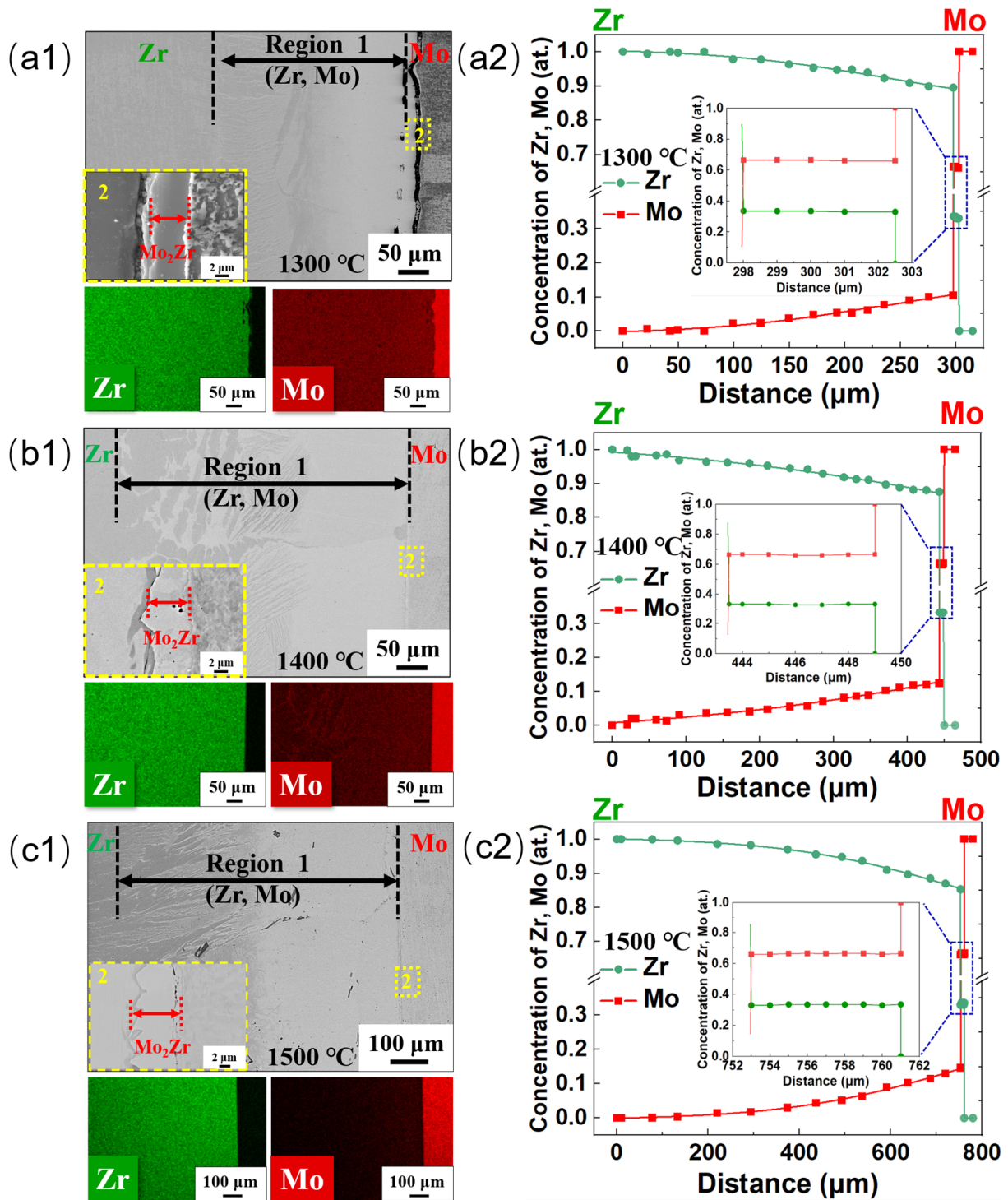
Figure 2. BSE images and EDX mapping of the entire diffused regions in Zr-Mo systems and the concentration distribution curve in the solid solution region after annealing at 1300–1500 °C for 5 h: (**a1,a2**), 1300 °C; (**b1,b2**), 1400 °C; (**c1,c2**), 1500 °C. The dashed square region 2 in (**a1,b1,c1**) represents the local enlarged images.

The diffused regions of the Zr-Mo system annealed at 1400 °C and 1500 °C for 5 h are shown in Figure 2(b1,c1), respectively. The elemental distribution state was similar to those at 1300 °C, i.e., the (Zr, Mo) solid solution and Mo_2Zr were formed in the diffused region. The curves of concentration distribution of the solid solution phase and Mo_2Zr phase are shown in Figure 2(b2,c2), respectively. The solid solubility of Mo in Zr at (Zr, Mo) solid

solution increased with temperature. The maximum content of Mo in the solid solution phase was 12 at. % and 14 at. % at 1400 °C and 1500 °C, respectively. Furthermore, the thickness of each diffusion layer increased with the temperature. The statistical thickness of the diffusion layer at each temperature is listed in Table 1, and the thickness of each phase was measured 20 times at different locations to obtain the average thickness and standard deviation. When the diffused temperature remained at, 1300 °C, 1400 °C and 1500 °C, the thickness of (Zr, Mo) solid solution phase reached 297 μm, 443 μm, and 753 μm, respectively, and the thickness of Mo_2Zr phase layer was 4.48 μm, 5.62 μm and 7.20 μm, respectively. From the increment of the diffused distance with temperature, the increment from 1400 °C to 1500 °C was larger than that from 1300 °C to 1400 °C. The thickness of the (Zr, Mo) solid solution increased by ~300 μm when the diffusion temperature was increased from 1400 °C to 1500 °C, while the thickness increased by only ~150 μm when the temperature was increased from 1300 °C to 1400 °C. This indicates that the temperature had a significant effect on diffusion promotion.

Table 1. The thickness of the (Zr, Mo) solid solution phase and Mo_2Zr phase in the Zr-Mo binary system after diffusion for 5 h at 1300 °C, 1400 °C, and 1500 °C.

| T/°C | The Thickness of Each Diffusion Layer/μm | |
	(Zr, Mo) Solid Solution Phase	Mo_2Zr Phase
1300	297 ± 21	4.48 ± 0.11
1400	443 ± 30	5.62 ± 0.23
1500	753 ± 40	7.20 ± 0.47

3.1.2. Zr-W Binary System

Figure 3a shows the BSE image and EDX-mapping of the entire diffused region tested by EDX quantitative analysis for the Zr-W diffusion system after annealing at 1300 °C for 5 h. Different from the Zr-Mo system, the solid solution phase layer was not observed in the Zr-W system. This might be due to the higher activation energy of the solid solution phase in the Zr-W system, which required a higher temperature to be formed. The quantitative analysis of the diffused region by EDX indicated that there were three regions in the Zr-W system. Sequentially, they were pure Zr, W_2Zr phase, and pure W. The diffused regions of the Zr-W system annealed at 1400 °C and 1500 °C for 5 h are shown in Figure 3b and c, respectively. The elemental distribution state was similar to those at 1300 °C, i.e., the W_2Zr were formed in the diffused region. When the diffused time was the same, the thickness of the W_2Zr phase layer increased with the temperature, as shown in Table 2. At 1300 °C, 1400 °C, and 1500 °C, the thickness of the W_2Zr phase layer was 4.15 μm, 7.52 μm, and 14.22 μm, respectively.

Table 2. The thickness of W_2Zr after diffusion for 5 h at 1300–1500 °C.

	1300 °C	1400 °C	1500 °C
Thickness	4.15 ± 0.23 μm	7.52 ± 0.46 μm	14.22 ± 0.69 μm

The thickness of the W_2Zr layer was very thin and the increment with temperature was only a few microns. The thickness increased by ~7 μm when the diffusion temperature was increased from 1400 °C to 1500 °C, while it increased by only ~3.5 μm when the temperature increased from 1300 °C to 1400 °C. This was due to the high melting points of W (3410 °C) and Zr (1842 °C), which resulted in the weak ability of atomic migration under the heat activation effect. While the melting point of Mo (2610 °C) was lower than that of W, the Zr-Mo system required lower activation energy for diffusion. Moreover, the diffusion in the Zr-W system became multiphase diffusion of $W-W_2Zr-Zr$ as diffusion proceeded. The W_2Zr phase could be observed on the Zr side at all temperatures in this work, e.g., the image of the Zr side at 1500 °C shown in Figure 4. This was dominated by two processes: (i) the initial diffusion was also controlled by vacancy mechanism, the Zr

side could easily provide the vacancy for W atomic migration due to a lower melting point of Zr; and (ii) simultaneously, W_2Zr formed by the assistance of the diffusion and reaction under thermal driving effect.
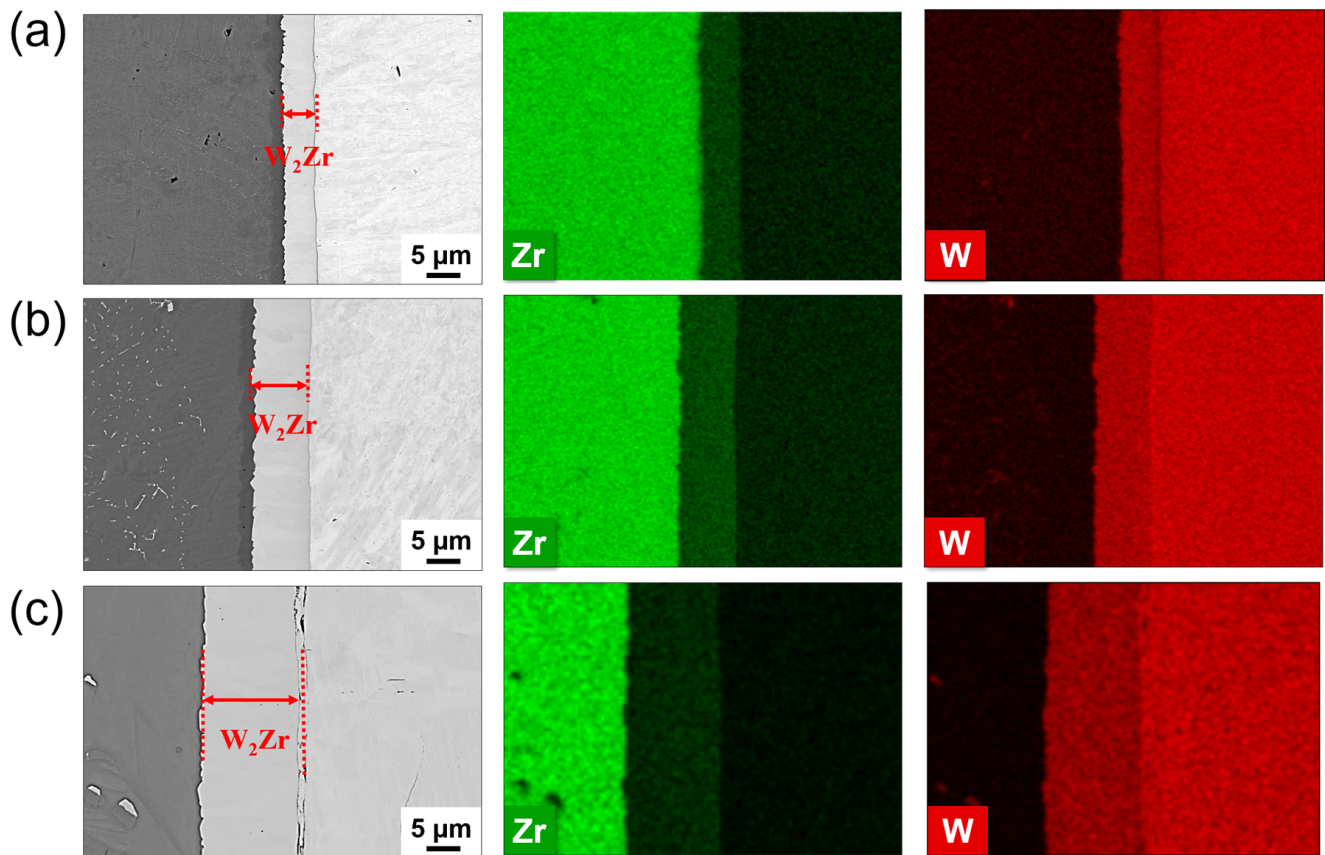

Figure 3. BSE images and EDX mapping of the entire diffused regions in Zr-W systems: (**a**), 1300 °C; (**b**), 1400 °C; (**c**), 1500 °C.
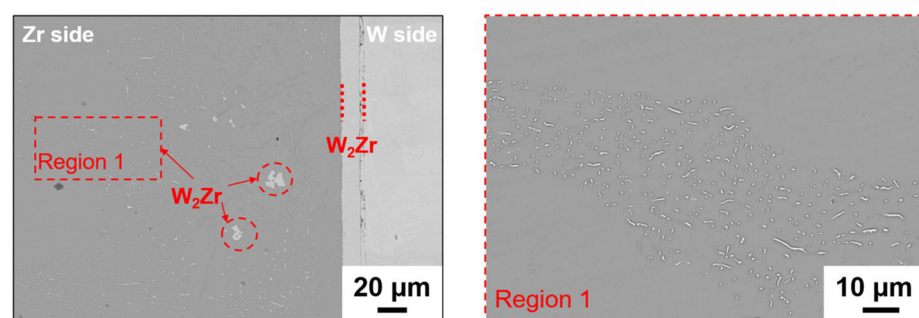

Figure 4. BSE image of Zr side in Zr-W system after diffusion at 1500 °C for 5 h.

As mentioned above, the interdiffusion region included the Mo_2Zr phase of only a few microns and the (Zr, Mo) solid solution phase of several hundred microns in the Zr-Mo system after diffusion at 1300–1500 °C as shown in Figure 5a, and the Mo content in the (Zr, Mo) solid solution was between 0 and 14 at. %, while the interdiffusion region only included the W_2Zr phase in the Zr-W system, as shown in Figure 5b.
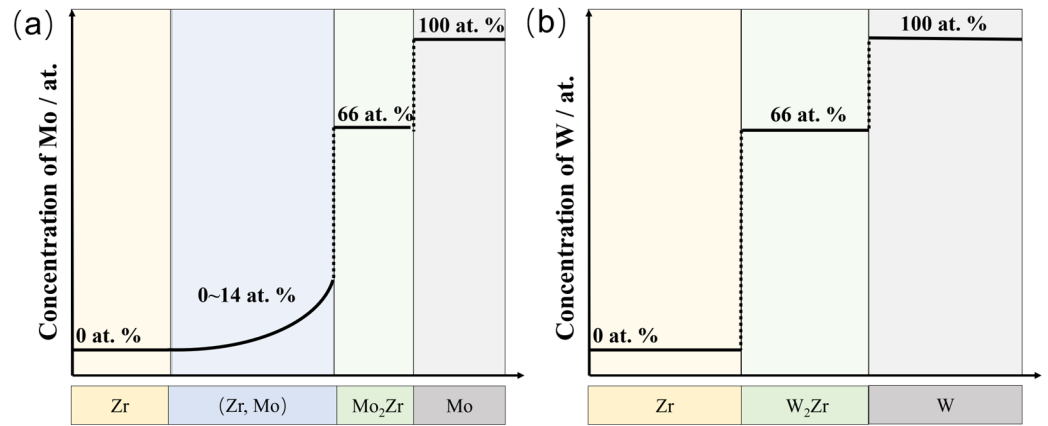
Figure 5. Schematic diagrams of the (**a**) Zr-Mo and (**b**) Zr-W diffusion region after diffusion at 1300–1500 °C.

3.2. Growth Kinetics of Mo_2Zr and W_2Zr

Assuming that the growth of the Mo_2Zr and W_2Zr phase was controlled by diffusion mechanism, the growth constants of the Mo_2Zr and W_2Zr phases could be calculated based on the thickness of the Mo_2Zr and W_2Zr layers at different temperatures combined with Equation (1) [25,26]:

$$K_p = \frac{x^2}{t} \tag{1}$$

where K_p is the parabolic growth constant, x is the thickness of the phase, and t is the diffused time. The calculated results are shown in Figure 6. At 1300 °C, 1400 °C, and 1500 °C, the growth constants of Mo_2Zr were 1.115×10^{-15} m^2/s, 1.755×10^{-15} m^2/s and 3.736×10^{-15} m^2/s, respectively, while the growth constants of W_2Zr were 9.56×10^{-16} m^2/s, 3.142×10^{-15} m^2/s, and 11.233×10^{-15} m^2/s, respectively. Mo_2Zr and W_2Zr had approximate growth constants at 1300 °C, while at 1400 °C and 1500 °C, W_2Zr had greater growth constants than Mo_2Zr.
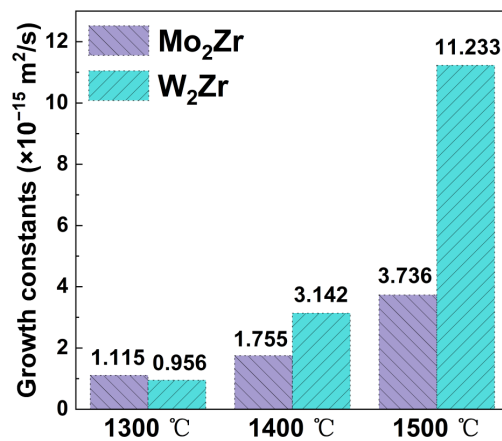

Figure 6. Growth constants of Mo_2Zr and W_2Zr ($\times 10^{-15}$ m^2/s).

To quantitatively calculate the activation energy for growth of the Mo_2Zr and W_2Zr phases, the growth constant versus temperature was obtained as shown in Figure 7, with lnK_p as the vertical coordinate and 10,000/T as the horizontal coordinate. The goodness of fit (r^2) in both Figure 7a,b were over 0.99, which indicates that the values of the growth constants at each temperature were in accordance with the Arrhenius relationship [20,27]:

$$lnK_p = lnK_0 - \frac{Q}{RT} \tag{2}$$

where Q is the activation energy of growth, T is the annealing temperature in Kelvin, R is the ideal gas constant, and K_0 is known as the pre-exponential factor. The intercept of the fitted line was lnK_0, and the slope was $-Q/R$. According to the slope and intercept of the fitted line in Figure 7, the pre-exponential factor and activation energy for the growth of the Mo_2Zr phase and W_2Zr phase can be calculated. The quantitatively calculated pre-exponential factors for the growth of Mo_2Zr and W_2Zr phases are 4.9×10^{-12} m^2/s and 2.7×10^{-6} m^2/s, respectively. The activation energies for the growth of the Mo_2Zr and W_2Zr phases are 109 kJ/mol and 285 kJ/mol, respectively.
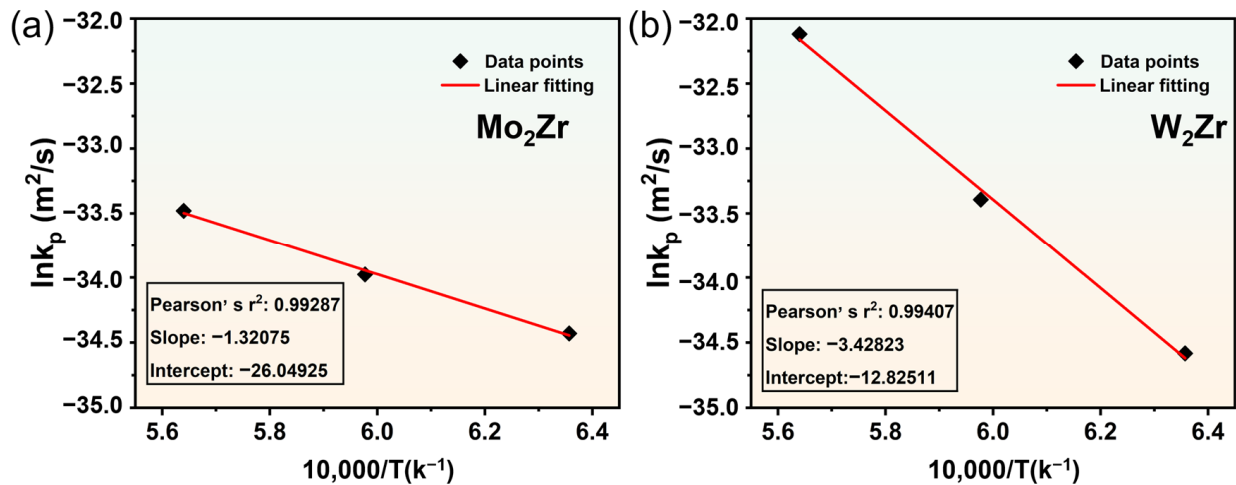

Figure 7. Temperature-dependence of growth constants calculated for Mo_2Zr and W_2Zr: (**a**) Mo_2Zr; (**b**) W_2Zr.

Although the activation energy for the growth of the W_2Zr phase was greater than that of the Mo_2Zr phase, the Mo_2Zr layer was thinner than that of the W_2Zr at 1400 °C and at 1500 °C, and the growth constant of the Mo_2Zr phase was less than that of W_2Zr phase. The reason behind this phenomenon can be explained as follows: (i) it is well known that the driving force of diffusion is the chemical potential gradient; (ii) Mo_2Zr was formed between pure Zr and pure Mo in the initial stage of diffusion, and as the diffusion proceeded, the (Zr, Mo) solid solution formed between pure Zr and Mo_2Zr, Mo_2Zr grew between the (Zr, Mo) solid solution and pure Mo in the late stage of diffusion; consequently, (iii) the chemical potential of the formation of the Mo_2Zr phase was reduced. In brief, (Zr, Mo) solid solution was formed between Mo_2Zr and pure Zr as diffusion proceeded, resulting in a decreased chemical potential for the formation of Mo_2Zr. Quantitative calculation of the kinetic parameters of diffusion in the (Zr, Mo) solid solution phase will be presented in the next section.

3.3. Interdiffusion Coefficient and Activation Energy of Diffusion in (Zr, Mo) Solid Solution Phase

Since a concentration gradient existed in the (Zr, Mo) solid solution, the interdiffusion coefficient could be calculated by solving Fick's second law. The concentration C at each part of the diffused region is related to the distance x and time t. Fick's second law revealed the relationship between C, x, and t [28]:

$$\frac{\partial C}{\partial t} = \frac{\partial}{\partial x}\left(\widetilde{D}\frac{\partial C}{\partial x}\right) \qquad (3)$$

Boltzmann and Matano successively proposed methods for calculating the interdiffusion coefficient by solving Fick's second law with experimentally measured concentration distribution curves and concentration gradients. However, this method caused some inaccuracies because it neglected the change in molar volume at different concentrations, so it should be modified. In this study, the den Broeder method based on the Boltzmann–

Matano model was used to calculate the interdiffusion coefficients. This method avoids the calculation error caused by the introduction of the Matano plane and also takes into account the change of the molar volume V_m owing to the change in the concentration of the components during the diffusion process [29]. The interdiffusion coefficient in the (Zr, Mo) solid solution phase was calculated based on the concentration distribution curve in Figure 2. The interdiffusion coefficient at the atomic concentration c* (abscissa x*) was expressed as [30,31]:

$$\widetilde{D}(c^*) = \frac{V_m}{2t} \left(\frac{d_x}{d_c} \right)_{c^*} \left[\left(\frac{c_2 - c^*}{c_2 - c_1} \right) \int_{-\infty}^{x^*} \frac{(c - c_1)}{V_m} dx + \left(\frac{c^* - c_1}{c_2 - c_1} \right) \int_{x^*}^{+\infty} \frac{(c_2 - c)}{V_m} dx \right] \quad (4)$$

where t is the diffusion time, c_1 and c_2 are respectively the atomic concentrations on both sides of the diffused region, and c represents the atomic concentration of Mo at position x. V_m is the molar volume of the concentration of the specific component, and since the Zr-Mo system is in the bcc phase region at experimental conditions in this work, V_m can be calculated as:

$$V_m(c_m) = N_0 \left[c_m \frac{a_m^3}{2} + (1 - c_m) \frac{a_z^3}{2} \right] \quad (5)$$

where N_0 is Avogadro's constant as 6.02×10^{23}; c_m is the molar fraction of the element Mo; a_m and a_Z are lattice parameters of the components Mo and Zr with bcc structure, respectively.

The concentration-dependent interdiffusion coefficients calculated from Equation (4) for the (Zr, Mo) solid solution phase in the range of 1300–1500 °C are shown in Figure 8. The interdiffusion coefficient of the (Zr, Mo) solid solution was between 1.5×10^{-13} m^2/s and 1.4×10^{-12} m^2/s at 1300–1500 °C, which was two magnitudes larger compared to the growth constant of the Mo$_2$Zr phase. Furthermore, the interdiffusion coefficient of the Zr-Mo system with the solid solution phase decreased with the increase of Mo content. At 1300 °C and Mo content of 0–10 at. %, the interdiffusion coefficient of (Zr, Mo) solid solution ranged from 1.5×10^{-13} m^2/s to 4×10^{-13} m^2/s; at 1400 °C and Mo content of 0–10 at. %, it ranged from 3.0×10^{-13} m^2/s to 8.0×10^{-13} m^2/s; at 1500 °C and Mo content of 0–10 at. %, it ranged from 2.8×10^{-13} m^2/s to 1.4×10^{-12} m^2/s. In general, the interdiffusion coefficient showed concentration dependence.
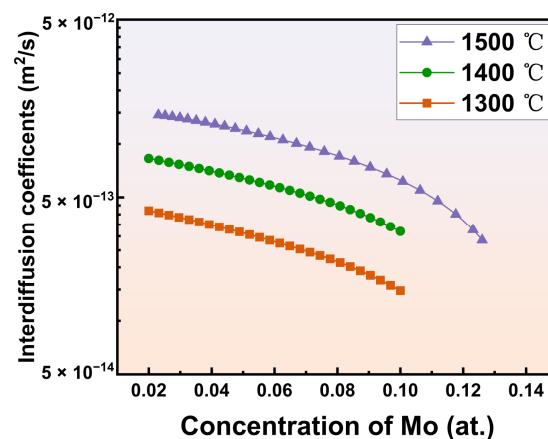

Figure 8. The relationship between concentration and interdiffusion coefficient in (Zr, Mo) solid solution phase.

Once the interdiffusion coefficients at each temperature were obtained, the activation energy of diffusion was calculated based on the linear relationship of the Arrhenius equation, lnD = f(1/T). The values of the activation energy and pre-exponential factor were illustrated in Figure 9 and Table 3, respectively. The activation energy of diffusion of the solid solution phase in the Zr-Mo system increased with the increase of Mo content. The activation energy of diffusion was 145–170 kJ/mol when the Mo content was in the range of 2–10 at. %. Although the activation energy of Mo$_2$Zr phase growth was less than the

activation energy of diffusion in the (Zr, Mo) solid solution, the growth constant of the Mo_2Zr phase was much less than the interdiffusion coefficient in the (Zr, Mo) solid solution. Therefore, the thickness of the Mo_2Zr phase layer was less than that of the (Zr, Mo) solid solution. In addition, the complex cubic structure of Mo_2Zr crystals was also a factor that affected the formation and growth of the Mo_2Zr phase [20].
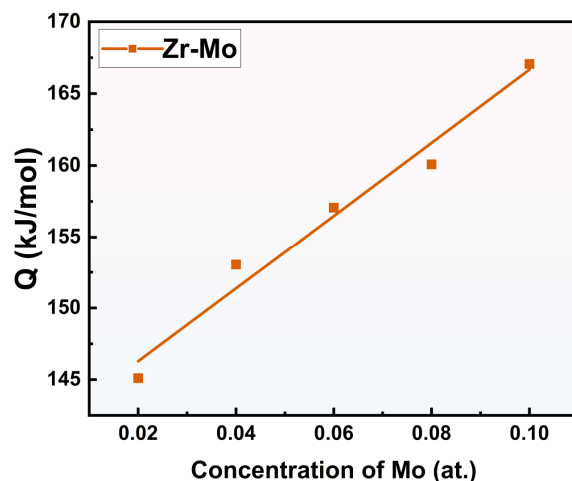

Figure 9. Activation energy corresponding to different concentrations of elements in (Zr, Mo) solid solution phase.

Table 3. Pre-exponential factors D_0 at different Mo element concentrations.

	0.02 at.	0.04 at.	0.06 at.	0.08 at.	0.1 at.
$D_0/10^{-8}$ m^2s	2.779	4.207	4.607	4.481	5.231

4. Conclusions

In this paper, the interdiffusion behavior of the Zr-Mo and Zr-W binary systems at 1300 °C, 1400 °C, and 1500 °C was systematically investigated by the solid–solid diffusion couple. The conclusions are as follows:

1. For the Zr-Mo binary system, the (Zr, Mo) solid solution phase with concentration gradient and Mo_2Zr phase were formed in the diffused region at 1300–1500 °C. At 1300 °C, 1400 °C, and 1500 °C, the thickness of the (Zr, Mo) solid solution was 297 μm, 443 μm, and 753 μm, respectively. The thickness of the Mo_2Zr was 4.48 μm, 5.62 μm, and 7.20 μm, respectively. For the Zr-W binary system, the W_2Zr phase was formed in the diffused region. At 1300 °C, 1400 °C, and 1500 °C, the thickness of the W_2Zr was 4.15 μm, 7.52 μm, and 14.22 μm, respectively.

2. The growth constants of Mo_2Zr and W_2Zr with temperature in accordance with the Arrhenius relationship, and the calculated activation energy of Mo_2Zr and W_2Zr phase growth was 109 kJ/mol and 285 kJ/mol, respectively.

3. In the diffusion process of the Zr-Mo system, the formation of (Zr, Mo) solid solution resulted in a decreased chemical potential for the formation of Mo_2Zr. The interdiffusion coefficient of the (Zr, Mo) solid solution phase showed concentration dependence, which decreased with the increase of Mo content. Additionally, the activation energy of diffusion of the (Zr, Mo) solid solution phase was 145–170 kJ/mol at a Mo content of 2–10 at. %.

Institutional Review Board Statement: Not applicable.

Informed Consent Statement: Not applicable.

Data Availability Statement: Data will be made available on request.

Conflicts of Interest: The authors declared that they have no conflict of interest in this work.

References

1. Daniel, C.S.; Garner, A.; Honniball, P.D.; Bradley, L.; Preuss, M.; Prangnell, P.B.; da Fonseca, J.Q. Co-deformation and dynamic annealing effects on the texture development during alpha-beta processing of a model Zr-Nb alloy. *Acta Mater.* **2021**, *205*, 116538. [CrossRef]
2. Suyalatu; Kondo, R.; Tsutsumi, Y.; Doi, H.; Nomura, N.; Hanawa, T. Effects of phase constitution on magnetic susceptibility and mechanical properties of Zr-rich Zr-Mo alloys. *Acta Biomater.* **2011**, *7*, 4259–4266. [CrossRef] [PubMed]
3. Wu, S.H.; Hou, Z.Q.; Zhang, J.Y.; Wang, Y.Q.; Wu, K.; Liu, G.; Sun, J. Understanding the strength softening of Zr/Mo and Zr/Ti nanostructured multilayers. *Scr. Mater.* **2019**, *172*, 61–65. [CrossRef]
4. Yang, H.L.; Shen, J.J.; Matsukawa, Y.; Satoh, Y.; Kano, S.; Zhao, Z.S.; Li, Y.F.; Li, F.; Abe, H. Effects of alloying elements (Sn, Nb, Cr, and Mo) on the microstructure and mechanical properties of zirconium alloys. *J. Nucl. Sci. Technol.* **2015**, *52*, 1162–1173. [CrossRef]
5. Nomura, S.N.; Oya, K.; Tanaka, Y.; Kondo, R.; Doi, H.; Tsutsumi, Y.; Hanawa, T. Microstructure and magnetic susceptibility of as-cast Zr-Mo alloys. *Acta Biomater.* **2010**, *6*, 1033–1038. [CrossRef]
6. Ren, H.L.; Liu, X.J.; Ning, J.G. Microstructure and mechanical properties of W-Zr reactive materials. *Mater. Sci. Eng. A Struct. Mater. Prop. Microstruct. Process.* **2016**, *660*, 205–212. [CrossRef]
7. Le Claire, A.D. Diffusion in metals. *Prog. Met. Phys.* **1953**, *4*, 265–332. [CrossRef]
8. Si, S.P.; He, C.; Liu, S.; Fan, B.J.; Xie, R.Y.; Xue, X.Y.; Liu, J.X. Influence of impact velocity on impact-initiated reaction behavior of Zr-Ti-Nb alloy. *Mater. Des.* **2022**, *220*, 110846. [CrossRef]
9. Mehrer, H. Irreversible Thermodynamics and Diffusion. In *Diffusion in Solids: Fundamentals, Methods, Materials, Diffusion-Controlled Processes*; Springer: Berlin/Heidelberg, Germany, 2007; pp. 191–206. [CrossRef]
10. Mehrer, H. Diffusion in Dilute Substitutional Alloys. In *Diffusion in Solids: Fundamentals, Methods, Materials, Diffusion-Controlled Processes*; Springer: Berlin/Heidelberg, Germany, 2007; pp. 327–339. [CrossRef]
11. Patil, R.V.; Kale, G.B.; Garg, S.P. Chemical diffusion in Zr-Nb system. *J. Nucl. Mater.* **1995**, *223*, 169–173. [CrossRef]
12. Liu, Y.J.; Zhang, L.J.; Pan, T.Y.; Yu, D.; Ge, Y. Study of diffusion mobilities of Nb and Zr in bcc Nb-Zr alloys. *Calphad* **2008**, *32*, 455–461. [CrossRef]
13. Zee, R.H.; Watters, J.F.; Davidson, R.D. Diffusion and chemical activity of Zr-Sn and Zr-Ti systems. *Phys. Rev. B* **1986**, *34*, 6895–6901. [CrossRef] [PubMed]
14. Thibon, I.; Ansel, D.; Gloriant, T. Interdiffusion in β-Ti-Zr binary alloys. *J. Alloys Compd.* **2009**, *470*, 127–133. [CrossRef]
15. Araki, H.; Minamino, Y.; Yamane, T.; Nakatsuka, T.; Miyamoto, Y. Pressure dependence of anomalous diffusion of zirconium in beta-titanium. *Metall. Mater. Trans. A Phys. Metall. Mater. Sci.* **1996**, *27*, 1807–1814. [CrossRef]
16. Ansel, D.; Margottet, A.; Boliveau, M.; Debuigne, J. Interdiffusion in the high temperature BCC beta Hf-Zr solid-solution. *Scr. Mater.* **1996**, *34*, 749–755. [CrossRef]
17. Zhang, J.; Gadelmeier, C.; Sen, S.; Wang, R.; Zhang, X.; Zhong, Y.; Glatzel, U.; Grabowski, B.; Wilde, G.; Divinski, S.V. Zr diffusion in BCC refractory high entropy alloys: A case of 'non-sluggish' diffusion behavior. *Acta Mater.* **2022**, *233*, 117970. [CrossRef]
18. Wang, J.; Fang, L.Y.; Li, X.N.; Liu, F.L.; He, X.C.; Xu, G.L.; Zhou, Y.L.; Tao, X.M.; Ouyang, Y.F.; Du, Y. Interdiffusion behaviors and mechanical properties of Zr-X (X=Nb, Ta, Hf) binary systems. *J. Alloys Compd.* **2022**, *910*, 10. [CrossRef]
19. Prasad, S.; Paul, A. Interdiffusion in Nb-Mo, Nb-Ti and Nb-Zr systems. In *Defect and Diffusion Forum*; Trans Tech Publications Ltd.: Stafa-Zurich, Switzerland, 2012; Volume 323/325. [CrossRef]
20. Puente, A.P.Y.; Dickson, J.; Keiser, D.D.; Sohn, Y.H. Investigation of interdiffusion behavior in the Mo-Zr binary system via diffusion couple studies. *Int. J. Refract. Met. Hard Mater.* **2014**, *43*, 317–321. [CrossRef]
21. Xing, L.N.; Liu, X.W.; Cao, Z.M.; He, C.; Liu, J.X. Effect of increasing Ti content on the phase, interface, dynamic mechanical properties and ballistic performance of W-Ti-Zr alloys. *Mater. Sci. Eng. Struct. Mater. Prop. Microstruct. Process.* **2022**, *831*, 142196. [CrossRef]
22. Morais, N.W.S.; Schon, C.G. Mechanical characterization of U-9Mo-3Zr and U-3Mo-9Zr alloys. *J. Alloys Compd.* **2021**, *871*, 159501. [CrossRef]
23. Zhou, F.Y.; Wang, B.L.; Qiu, K.J.; Li, L.; Lin, J.P.; Li, H.F.; Zheng, Y.F. Microstructure, mechanical property, corrosion behavior, and in vitro biocompatibility of Zr-Mo alloys. *J. Biomed. Mater. Res. Part B Appl. Biomater.* **2013**, *101*, 237–246. [CrossRef]
24. Chang, Y.A. Phase investigations in the system zirconium-tungsten. *J. Less Common Met.* **1969**, *17*, 325–328. [CrossRef]

25. Zhuang, R.J.; Tan, Y.K.; Liu, Y.; Tao, X.M.; Chen, H.M.; Ouyang, Y.F.; Du, Y. Interdiffusion behaviors and mechanical properties of Zn-Cr system. *Calphad-Comput. Coupling Ph. Diagr. Thermochem.* **2021**, *74*, 102308. [CrossRef]

26. Wagner, C. Evaluation of data obtained with diffusion couples of binary single-phase and multiphase systems. *Acta Metall.* **1969**, *17*, 99–107. [CrossRef]

27. Darken, L.S. Diffusion, mobility and their interrelation through free energy in binary metallic systems. *Trans. Am. Inst. Min. Metall. Pet. Eng.* **1948**, *175*, 184–201. [CrossRef]

28. Mehrer, H. Diffusion and External Driving Forces. In *Diffusion in Solids: Fundamentals, Methods, Materials, Diffusion-Controlled Processes*; Springer: Berlin/Heidelberg, Germany, 2007; pp. 179–190. [CrossRef]

29. Wu, X.K.; Zhong, J.; Zhang, L.J. A general approach to quantify the uncertainty of interdiffusion coefficients in binary, ternary and multicomponent systems evaluated using Matano-based methods. *Acta Mater.* **2020**, *188*, 665–676. [CrossRef]

30. Broeder, F. A general simplification and improvement of the matano-boltzmann method in the determination of the interdiffusion coefficients in binary systems. *Scr. Metall.* **1969**, *3*, 321–325. [CrossRef]

31. Ahmed, T.; Belova, I.; Evteev, A.; Levchenko, E.; Murch, G. Comparison of the Sauer-Freise and Hall Methods for Obtaining Interdiffusion Coefficients in Binary Alloys. *J. Phase Equilib. Diffus.* **2015**, *36*, 366–374. [CrossRef]